Supplementary Materials

Enhanced Photocatalytic Nitrogen Fixation over MnO_x-Modified O-$KNbO_3$: Impact of Oxygen Vacancies and MnO_x Loading

Chuanqi Xia [a,‡], Jinying Teng [d, ‡], Lin Yue[a], Yekang Zheng [b], Yuxing Chu [b], Lvchao Zhuang [b, *], Leihong Zhao [a, c*], Yiming He [a, b, c*]

[a] *Key Laboratory of the Ministry of Education for Advanced Catalysis Materials, Institute of Physical Chemistry, Zhejiang Normal University, Jinhua, 321004, China*

[b] *Department of Material Science and Engineering, Zhejiang Normal University, Jinhua, 321004, China*

[c] *College of Jewelry, Shanghai Jianqiao University, Shanghai, 201306, China*

[d] *School of Science, Xi'an Jiaotong-Liverpool University, Suzhou 215123, China*

‡These authors contributed equally to this work.

Corresponding author:

E-mail: lyuchao.zhuang@zjnu.edu.cn (L. Chao); zhaoleihong@163.com (L. Zhao); hym@zjnu.cn (Y. He)

1. Preparation of catalysts

$KNbO_3$ was synthesized via a hydrothermal method. First, 44.8 g of KOH was dissolved in 60 ml of distilled water to form a clear solution. Then, 2.6581 g of Nb_2O_5 was added to the solution and stirred for 0.5 h. The mixture was transferred into a Teflon-lined autoclave and reacted at 200 °C for 24 h. After cooling to room temperature, the product was centrifuged and washed three times with distilled water and ethanol. The obtained product was dried at 60 °C for 12 h to yield cubic $KNbO_3$ blocks.

2. Photocatalytic N_2 fixation reaction

The photocatalytic nitrogen fixation experiments were conducted in a self-built photochemical reactor. A 300W Xe lamp (PLS-SXE300C, Beijing ProfectLight Co. Ltd., China) was used as the simulated sunlight source (350-980 nm). The distance between the xenon lamp and the reactor was set to 10 cm, and the light intensity at the reactor was about 100 mW/cm^2. A UV-cut filter (λ>420 nm) was applied during the visible-light-driven photocatalytic reaction, resulting in a reduced light intensity of approximately 70 mW/cm^2. Prior to light irradiation, 0.05 g of solid catalyst was added into a 100 mL methanol solution (containing 5 mL methanol and 95 mL deionized water) and stirred for 1 h in the dark to ensure an adsorption–desorption equilibrium. During light exposure, 7 mL of the liquid was extracted from the solution every one-hour interval for ammonia detection. The sample solution was centrifuged to obtain the supernatant, and then 30 μL of sodium tartrate and 30 μL of Nessler's reagent were added successively. After 12 min of reaction, the ammonia concentration was analyzed by measuring the absorbance at 420 nm with a

UV-vis spectrophotometer. The photocatalytic N_2 fixation in the presence of different scavengers was conducted similarly, except that the scavenger was changed. For the reaction performed in the presence of N_2, the bubbling N_2 flow rate was controlled to 50 mL min^{-1}. For the reaction under vacuum, the reactor was replaced with a closed quartz reactor. After the reaction solution and catalyst were added, the air in the reactor was evacuated, and the relative pressure to the outside world was maintained at -97kPa (the actual pressure was about 4.3kPa). All photocatalytic reaction tests were conducted in triplicate to ensure the reliability of the results.

3. Determination of NH_3 content by the NMR method

After 5-hour photocatalytic reaction, the NH_4^+ content was quantitatively determined by ^1H nuclear magnetic resonance (NMR, 600 MHz, Bruker AV600) with external standards, taking maleic acid ($C_4H_4O_4$) as a reference. To create the calibration curve, a series of NH_4^+ solutions with known concentration were prepared in 0.01 M HCl as standards. Next, 24.5 mL of the NH_4^+ standard solution was mixed with 0.5 mL maleic acid (25 μg/mL). The mixture was then concentrated to approximately 1 mL and identified using ^1H NMR spectroscopy (50 μL deuterium oxide (D_2O) was added in 0.45 mL concentrated solution before NMR detection). The calibration was achieved using the peak area ratio between NH_4^+ and tris-maleate because the NH_4^+ concentration and the area ratio are positively correlated. Similarly, the NH_4^+ concentration after photocatalytic reaction was quantitatively determined using this method.

4. Characterizations of catalysts

X-ray diffraction (XRD) analysis was performed on a D8 Advance (BRUKER AXS GMBH,

Germany) X-ray diffractometer using Cu Kα radiation (40 kV/40 mA). X-ray fluorescence (XRF) spectrometer (SHIMADZU EDX-GP) was used to analyze the Mn element in MnO_x/O-$KNbO_3$ catalyst. Raman spectra of the MnO_x/O-$KNbO_3$ catalysts were recorded on a RM1000 spectrometer (Renishaw) via an excitation source of an Ar ion laser (514.5 nm). UV-visible diffuse reflection spectroscopy (DRS) was actualized on a UV-visible spectrophotometer (Agilent Cary5000) and the reference sample was $BaSO_4$. Scanning electron microscopy (SEM) was carried out on a Field emission scanning electron microscope (Hitachi S-4800) with the accelerating voltage of 5 kV. Transmission electron microscopy (TEM) was employed on a JEM-2010F transmission electron microscope via the accelerating voltage of 200 kV. The X-ray photoelectron spectroscopy (XPS) spectra of the catalysts were obtained via using a Thermo Scientific ESCALAB 250Xi Microprobe instrument using Al-Kα as a ray source. The C 1s signal was adjusted in the location of 284.6 eV. Ultraviolet photoelectron spectroscopy (UPS) analysis was performed on the same instrument using a He lamp (HeI line, 21.22 eV) as the light source. A CHI 660E electrochemical workstation with a standard three-electrode cell was employed to perform the photocurrent responses, linear sweep voltammetry (LSV), and the electrochemical impedance spectroscopy (EIS). The test was operated at room temperature. The piezocatalyst, Ag/AgCl (saturated KCl), and a Pt wire were used as the working electrode, the reference electrode, and the counter electrode, respectively. The ESR spectra were recorded at room temperature using a Bruker model ESR JES-FA200 spectrometer. Photoluminescence (PL) spectra of the catalyst were recorded on an FLS-920 fluorescence spectrometer manufactured by Edinburgh-Instrument, UK. Surface photovoltage (SPV) analysis was conducted on a steady-state surface photovoltage spectrometer (PL-SPV/IPCE1000, PerfectLight Technology).

5. Theoretical models and method

First-principles calculations based on density functional theory were implemented by the Vienna ab initio simulation package (VASP)[G. Kresse and J. Hafner, Phys Rev B, 1994, 49, 14251-14269. J. Hafner, J Comput Chem, 2008, 29, 2044-2078]. The Perdew-Burke-Ernzerhof (PBE) [John P. Perdew, Kieron Burke and M. Ernzerhof, Phys Rev Lett, 1996, 77, 3865-3868] functional was used to calculate the electron exchange and correlation effects via the generalized gradient approximation (GGA) [J. P. Perdew and Y. Wang, Phys Rev B, 1992, 45, 13244-13249]. The projector augmented plane wave (PAW) method with a frozen-core approximation was used to describe electron-ion interaction [P. E. Blöchl, Phys Rev B, 1994, 50, 17953-17979]. The $3s^2 3p^6 4s^1$, $4s^2 4p^6 4d^4 5s^1$ and $2s^2 2p^4$ of K, Nb, and O atoms were treated as valence electrons, respectively. Special k-points constructed via the Monkhorst-Pack method were applied to sample the Brillouin zone.[H. J. Monkhorst and J. D. Pack, Phys Rev B, 1976, 13, 5188-5192]. The electronic structure calculations employed a 0.05 eV Gaussian smearing width and a 400 eV plane-wave cutoff energy, determined through convergence tests. The Kohn-Sham equations were solved self-consistently with an energy convergence criterion of 1.0×10^{-5} eV, while structural optimizations were performed until the maximum Hellmann-Feynman forces reached below 0.03 eV/Å.

The lattice constants of a, b and c for $KNbO_3$ optimized in the present work are 5.705, 5.724 and 3.970 Å with α=β=γ=90o, respectively. The N_2 adsorption was studied using three-layer O-K-Nb-O $KNbO_3$(111) p(1×1) slabs with and without oxygen vacancies, where the bottom layer was

fixed during optimization. A 15 Å vacuum layer was applied along the z-axis to prevent slab interactions. The O-terminated (111) surface was selected for its thermodynamic stability.

The adsorption energies of N_2 on $KNbO_3$ surfaces were defined as follows：

$$E_{ads} = E_{adsorbate/slab} - (E_{adsorbate} + E_{slab}),$$

where $E_{adsorbate/slab}$, E_{slab} and $E_{adsorbate}$ are the energies of the system, slab and free adsorbate, respectively. The negative adsorption energy means an exothermic adsorption. The more negative adsorption energy represents the stronger interaction between adsorbates and catalysts.

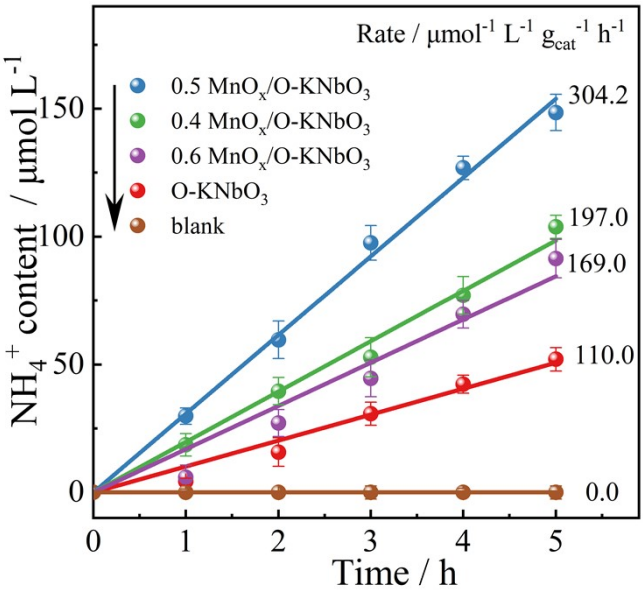

Fig. S1 Catalytic activity of different MnO_x/O-$KNbO_3$ samples in photocatalytic N_2 fixation. (The notation "0.5 MnO_x/O-$KNbO_3$" indicates a molar ratio of Mn to Nb of 0.5 during catalyst preparation. Similarly, the molar ratios for other samples are represented in the same manner)

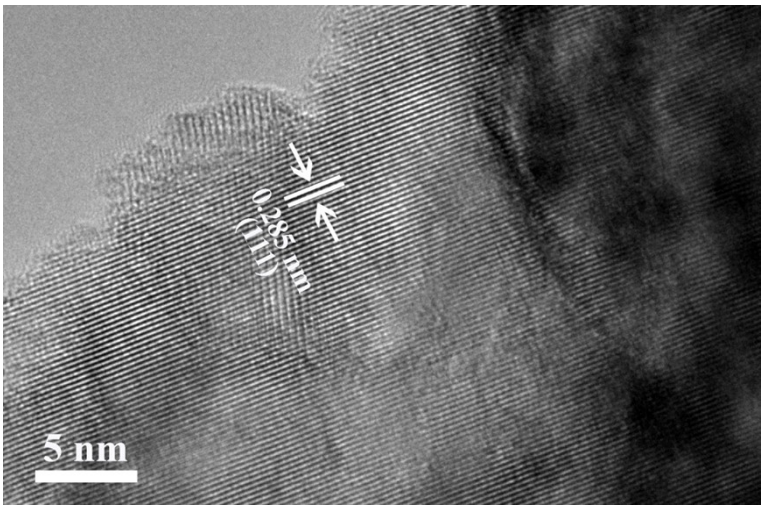

Fig. S2 HR-TEM image of pure $KNbO_3$

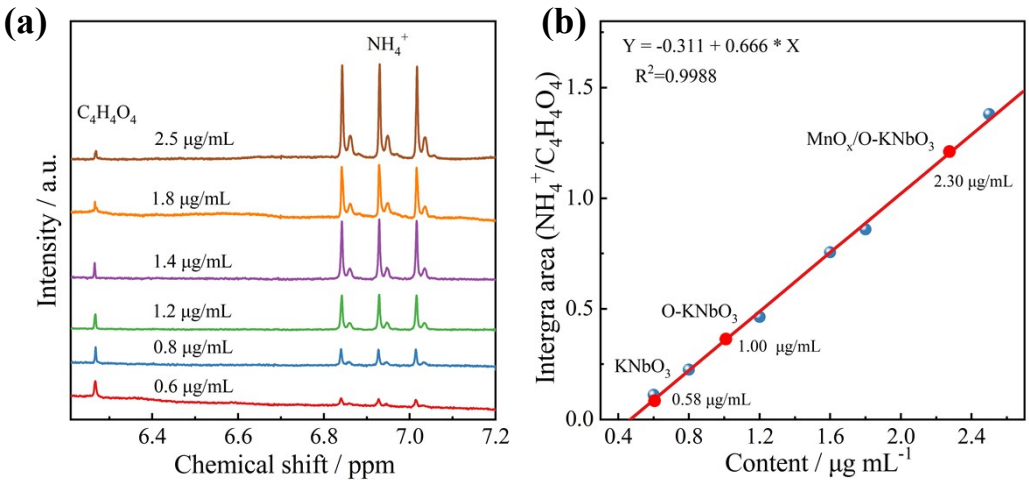

Fig. S3 ^{1}H NMR spectra (600 MHz) of various $^{14}NH_4^+$ solutions (a) and the standard curve line obtained via the external standard method (b).

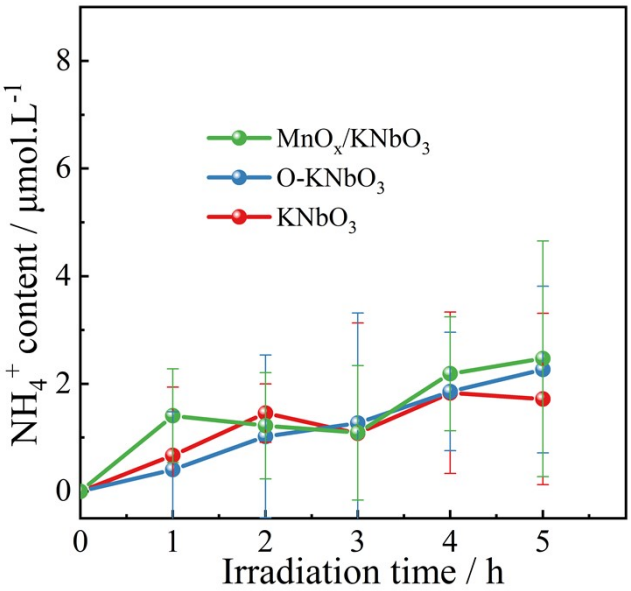

Fig. S4 Photocatalytic N_2 fixation activity of $KNbO_3$, O-$KNbO_3$, and MnO_x/O-$KNbO_3$ samples under visible light irradiation.

Table S1 Element concentrations in $KNbO_3$, O-$KNbO_3$, and MnO_x/O-$KNbO_3$ samples via XRF

Samples	Atomic content /%			Mn/Nb
	K	Nb	Mn	
$KNbO_3$	46.8%	53.2%%	-	
O-$KNbO_3$	47.4%	52.6%	-	
MnO_x/O-$KNbO_3$	44.0%	54.8%	1.2%	2.2%

Table S2 Summary of some metal titanates and composite catalysts for the N_2 reduction to NH_3

Catalyst	Nitrogen source	Sacrificial agent	NH_3 generation rate/μmol $L^{-1}g^{-1}h^{-1}$		Light source	Ref.
			Nessler method	NMR method		
$BiOBr/Ti_3C_2$	N_2		234	-	300 W	[1]
$NiS/KNbO_3$	air	CH_3CH_2OH	155.6	-	300 W	[2]
C-ZnO/MoS_2	air	CH_3CH_2OH	245		300W	[3]
N-graphyne/Bi/BiOBr	N_2	H_2O	56.8		300W	[4]
N-TiO_2/Ti_3C_2	N_2	H_2O	60.2		500W	[5]
$Fe_2Ti_2O_7$ film	N_2	CH_3CH_2OH	10[a]	-	UV[b]	[6]
$LaTiO_{3-x}$	N_2	CH_3OH	-	358[c]	300 W	[7]
Fe-$SrMoO_4$	N_2	CH_3OH	93.1	-	300W	[8]
Ag/Bi_5O_7I	Air	CH_3OH	240	67	300W	[9]
Bi-$CdMoO_4$	Air	CH_3OH	590	272	300W	[10]
$Ag_2S/KTa_{0.5}Nb_{0.5}O_3$	Air	CH_3OH	155	131	300W	[11]
$CuS/KTa_{0.75}Nb_{0.5}O_3$	Air	CH_3OH	167	102	300W	[12]
$Bi_2S_3/KTa_{0.75}Nb_{0.5}O_3$	Air	CH_3OH	561	176	300W	[13]
Bi-$Bi_2O_3/KTa_{0.5}Nb_{0.5}O_3$	Air	CH_3OH	466	223	300W	[14]
$PtBi/KTa_{0.5}Nb_{0.5}O_3$	Air	CH_3OH	385	202	300W	[15]
Pt/O-$NaNbO_3$	Air	CH_3OH	293	231	300W	[16]
$Bi_2O_3/CdMoO_4$	Air	CH_3OH	323	247	300W	[17]
MnO_x/O-$KNbO_3$	Air	CH_3OH	304	270	300W	This work

a: umol/L; *b*: Hg lamp; *c*: ion chromatography method;

References:

[1]. Y. Fang, Y. Cao, B.H. Tan, Q.L. Chen, Oxygen and titanium vacancies in a BiOBr/MXene-Ti_3C_2 composite for boosting photocatalytic N_2 fixation. ACS Appl. Mater. Interfaces 2021, 13(36): 42624-42634.

[2]. W.Q. Zhang, P.X. Xing, J.Y. Zhang, L. Chen, J.Y. Yang, X. Hu, L.H. Zhao, Y. Wu, Y.M. He, Facile preparation of novel nickel sulfide modified $KNbO_3$ heterojunction composite and its enhanced performance in photocatalytic nitrogen fixation. J. Colloid Interf. Sci. 2021, 590: 548–560

[3]. P.X. Xing, P.F. Chen, Z.Q. Chen, X. Hu, H.J. Lin, Y. Wu, L.H. Zhao, Y.M. He, Novel ternary MoS_2/C-ZnO composite with efficient performance in photocatalytic NH_3 synthesis under simulated sunlight. ACS Sustain. Chem. Eng. 2018, 6 (11): 14866–14879

[4]. X.Z. Huang, M.X. Sun, M. Humayun, S.Y. Li, J.J. Zhao, H.H. Chen, Z.Y. Li, In-situ synthesis of efficient N-graphyne/Bi/BiOBr photocatalysts for contaminants removal and nitrogen fixation. J. Alloys Compd. 2024, 976: 173025.

[5]. Z.P. Ding, M.X. Sun, W.Z. Liu, W.B. Sun, X.L. Meng, Z.Q. Zheng, Ultrasonically synthesized N-TiO_2/Ti_3C_2 composites: Enhancing sonophotocatalytic activity for pollutant degradation and nitrogen fixation, Sep. Purif. Technol. 2021, 276: 119287

[6]. H. Kisch, In the Light and in the Dark: Photocatalytic Fixation of Nitrogen into Ammonia and Nitrate at Iron Titanate Semiconductor Thin Films, Eur. J. Inorg. Chem. 2020, 15-16: 1376−1382

[7]. M.Y. Xia, B. Chong, X.J. Gong, H. Xiao, H. Li, H.H. Ou, B. Zhang, G.D. Yang, Ti^{2+} Site-Promoted N≡N Bond Activation in $LaTiO_{3-x}$ Nanosheets for Nitrogen Photofixation, ACS Catal. 2023, 13: 12350–12362

[8]. J.Y. Luo, X.X. Bai, Q. Li, X. Yu, C.Y. Li, Z.N. Wang, W.W. Wu, Y.P. Liang, Z.H. Zhao, H. Liu, Band structure engineering of bioinspired Fe doped $SrMoO_4$ for enhanced photocatalytic nitrogen reduction performance, Nano Energy 2019, 66: 104187.

[9]. L. Chen, W.Q. Zhang, J.F. Wang, X.J. Li, Y. Li, X. Hu, L.H. Zhao, Y. Wu, Y.M. He, High piezo/photocatalytic efficiency of Ag/Bi_5O_7I nanocomposite using mechanical and solar energy for N_2 fixation and methyl orange degradation, Green Energy Environ. 2023, 8: 283-295

[10]. J.F. Wang, L.F. Guan, S.D. Yuan, J.Y. Zhang, C.R. Zhao, X. Hu, B.T. Teng, Y. Wu, Y.M. He, Greatly boosted photocatalytic N_2-to-NH_3 conversion by bismuth doping in $CdMoO_4$: Band structure engineering and N_2 adsorption modification, Sep. Purif. Technol. 2023, 314:123554

[11]. L. Chen, J.F. Wang, X.J. Li, J.Y. Zhang, C.R. Zhao, X. Hu, H.J. Lin, L.H. Zhao, Y. Wu, Y.M. He, Facile preparation of $Ag_2S/KTa_{0.5}Nb_{0.5}O_3$ heterojunction for enhanced performance in catalytic nitrogen fixation via photocatalysis and piezo-photocatalysis, Green Energy Environ. 2023, 8: 1630−1643.

[12]. X.Q. Dai, L. Chen, Z.Y. Li, X.J. Li, J.F. Wang, X. Hu, L.H. Zhao, Y.M. Jia, S.X. Sun, Y. Wu, Y.M. He, $CuS/KTa_{0.75}Nb_{0.25}O_3$ nanocomposite utilizing solar and mechanical energy for catalytic N_2 fixation, J. Colloid Interf. Sci. 2021, 603:220−232.

[13]. L. Chen, X.Q. Dai, X.J. Li, J.F. Wang, H.F. Chen, X. Hu, H.J. Lin, Y.M. He, Y. Wu, M.H. Fan, Novel $Bi_2S_3/KTa_{0.75}Nb_{0.25}O_3$ nanocomposite with high efficiency for photocatalytic and

piezocatalytic N_2 fixation. J. Mater. Chem. A 2021, 9: 13344–13354.

[14]. L. Chen, J.F. Wang, X.J. Li, C.R. Zhao, X. Hu, Y. Wu, Y.M. He, A novel Z-scheme Bi-$Bi_2O_3/KTa_{0.5}Nb_{0.5}O_3$ heterojunction for efficient photocatalytic conversion of N_2 to NH_3, Inorg. Chem. Front. 2022, 9: 2714–2724.

[15]. X.J. Li, L. Chen, J.F. Wang, J.Y. Zhang, C.R. Zhao, H.J. Lin, Y. Wu, Y.M. He, Novel platinum-bismuth alloy loaded $KTa_{0.5}Nb_{0.5}O_3$ composite photocatalyst for effective nitrogen-to-ammonium conversion, J. Colloid Interf. Sci. 2022, 618: 362–374.

[16]. J.Y. Zhang, L. Yue, Z.H. Zeng, C.R. Zhao, L.J. Fang, X. Hu, H.J. Lin, L.H. Zhao, Y.M. He, Preparation of $NaNbO_3$ microcube with abundant oxygen vacancies and its high photocatalytic N_2 fixation activity in the help of Pt nanoparticles, J. Colloid Interf. Sci. 2023, 636: 480–491.

[17]. S.D. Yuan, J.F. Wang, C.R. Zhao, L. Yue, X.J. Ren, Z.H. Zeng, X. Hu, Y. Wu, Y.M. He, S-scheme $Bi_2O_3/CdMoO_4$ Hybrid with Highly Efficient Charge Separation for Photocatalytic N_2 fixation and Tetracycline Degradation: Fabrication, Catalytic Optimization, Physicochemical Studies, Sep. Purif. Technol. 2023, 325: 124665